Acta Crystallographica Section F
Structural Biology and Crystallization Communications
ISSN 1744-3091

Structure of *Francisella tularensis* peptidyl-tRNA hydrolase

Teresa E. Clarke,[a,b] Vladimir Romanov,[a,b] Robert Lam,[a,b] Scott A. Gothe,[c] Srinivasa R. Peddi,[c] Ekaterina B. Razumova,[b] Richard S. A. Lipman,[c] Arthur A. Branstrom[c] and Nickolay Y. Chirgadze[a,b,d]*

[a]Division of Cancer Genomics and Proteomics, Ontario Cancer Institute, University Health Network, MBRC 5th Floor, 200 Elizabeth Street, Toronto, Ontario M5G 2C4, Canada, [b]NEXTEX Technologies Inc., Toronto, Ontario M4N 1W6, Canada, [c]PTC Therapeutics Inc., 100 Corporate Court, South Plainfield, NJ 07080-2449, USA, and [d]Department of Pharmacology and Toxicology, University of Toronto, 1 King's College Circle, Toronto, Ontario M5S 1A8, Canada

Correspondence e-mail: nchirgad@uhnresearch.ca

Received 12 January 2011
Accepted 11 February 2011

PDB Reference: peptidyl-tRNA hydrolase, 3nea.

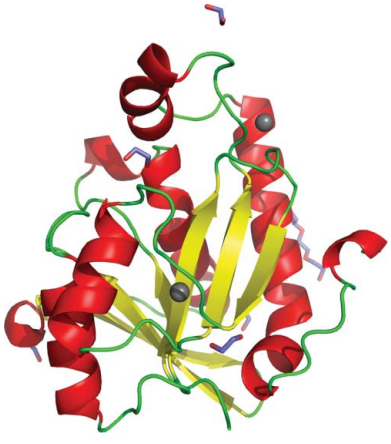

The rational design of novel antibiotics for bacteria involves the identification of inhibitors for enzymes involved in essential biochemical pathways in cells. In this study, the cloning, expression, purification, crystallization and structure of the enzyme peptidyl-tRNA hydrolase from *Francisella tularensis*, the causative agent of tularemia, was performed. The structure of *F. tularensis* peptidyl-tRNA hydrolase is comparable to those of other bacterial peptidyl-tRNA hydrolases, with most residues in the active site conserved amongst the family. The resultant reagents, structural data and analyses provide essential information for the structure-based design of novel inhibitors for this class of proteins.

1. Introduction

Francisella tularensis is a pathogenic species of Gram-negative bacteria and is the causative agent of tularemia or rabbit fever. *F. tularensis* is very infectious in that a small number of organisms (10–50) can cause disease (Oyston *et al.*, 2004). Owing to its ease of transmission by aerosol and its high virulence, *F. tularensis* has been classified as a Class A agent by the US government. Infection with *F. tularensis* can occur *via* several routes, including skin contact, inhalation, ingestion and inoculation of the eye. The bacteria that cause tularemia appear widely in nature and can be isolated and grown in culture, although producing an effective aerosol weapon would be difficult. Inhalation of an infectious aerosol would result in severe respiratory illness, including life-threatening pneumonia and systemic infection if left untreated. Although tularemia can be life-threatening, most infections can be treated successfully with antibiotics such as streptomycin, gentamicin, doxycycline and ciprofloxacin. However, given the organism's potential to be used as a bioterror agent, with antibiotic-resistance genes being engineered into strains, there is a need for new classes of antibiotics.

In an effort to discover novel antibiotics for Gram-negative bacteria such as *F. tularensis*, essential steps in the organism's protein-synthesis pathway have been identified as targets for potential interdiction. One such target arises during the process of protein translation, when a peptidyl-tRNA may dissociate prematurely from the ribosome before completion of mRNA decoding (Meinnel *et al.*, 1993; Schmitt *et al.*, 1997). Excess peptidyl-tRNA in cells leads to reduced efficiency of translation and eventually impairs translation initiation by cellular depletion of the required tRNA (Menninger, 1976, 1979). Peptidyl-tRNA hydrolase (Pth; EC 3.1.1.29) recycles peptidyl-tRNA by catalyzing the hydrolytic removal of the peptidyl moiety, allowing the reuse of the free tRNA in protein biosynthesis.

The enzyme Pth can be classified into two types: peptidyl-tRNA hydrolase 1 (Pth1) and peptidyl-tRNA hydrolase 2 (Pth2). Pth1 is found in bacteria and eukaryotes (Kössel, 1970; Brun *et al.*, 1971; Menez *et al.*, 2002), while Pth2 enzymes are present in eukaryotes and

Table 1
Summary of crystallographic data for *F. tularensis* Pth.

Values in parentheses are for the highest shell.

Data collection	
Wavelength (Å)	1.54
Resolution (Å)	50.0–2.25 (2.33–2.25)
Space group	$P2_12_12$
Unit-cell parameters	a = 60.7, b = 93.0, c = 33.0
Unique reflections	9412
Total no. of reflections	62322
Multiplicity	7
Completeness (%)	100 (100)
$\langle I/\sigma(I)\rangle$	14.4 (4.0)
$R_{\rm merge}$ (%)	14.0 (49.0)
Structure refinement	
No. of amino-acid chains	1
No. of protein atoms	
Main chain	758
Side chain	706
Total	1458
No. of solvent molecules	51
No. of other atoms	21
Resolution range (Å)	33.0–2.25
R factor (%)	19.0
$R_{\rm free}$ (%)	24.8
Average protein-chain B factor (Å^2)	
Main chain	24.3
Side chain	25.7
Total	25.0
Average solvent B factor (Å^2)	24.2
Average B factor for other atoms (Å^2)	34.3
R.m.s.d. covalent bond lengths (Å)	0.013
R.m.s.d. bond angles (°)	1.291
Missing residues	N-terminal hexahistidine tag, Met1

archaea (Rosas-Sandoval *et al.*, 2002; Fromant *et al.*, 2005). These two enzymes do not show any significant sequence identity or structural similarity. The first crystal structure of Pth1 from *Escherichia coli* (EcPth) revealed a single α/β globular domain built around a twisted mixed β-sheet (Schmitt *et al.*, 1997). The active site resides in a channel covered by a loop and short helix (α4) and contains the catalytic residues His20 (catalytic base) and Asp93 (Goodall *et al.*, 2004). The structure of *Mycobacterium tuberculosis* Pth (MtPth) revealed an open conformation of the peptide binding site of the enzyme and led to a model of structural changes associated with enzyme action, which was subsequently probed through a dynamics analysis utilizing MtPth solution structures (Selvaraj *et al.*, 2007; Pulavarti *et al.*, 2008). The first crystal structure of human Pth2 (hPth2; de Pereda *et al.*, 2004) showed a mixed β-sheet sandwiched by two groups of two α-helices and lacked any three-dimensional structural similarity to the structure of Pth1.

In this paper, we present the crystal structure of *F. tularensis* Pth (FtPth) at 2.25 Å resolution. Molecular modeling has indicated that there are two proximal sites for the potential binding of small molecules on either side of the His20 residue of EcPth in the crevice containing the active site (Pulavarti *et al.*, 2008). A structural comparison was used to determine residues unique to the binding site of FtPth which could be exploited for the development of antibacterial agents specific for *F. tularensis*.

2. Materials and methods

2.1. Cloning, protein expression and purification

The *F. tularensis* subspecies *tularensis* peptidyl-tRNA hydrolase (FTF0680c) gene encoding residues 1–188 was *Escherichia coli* optimized and synthesized by incorporating an *Nde*I restriction site at the N-terminus and an *Xho*I site at the C-terminus. The gene was subcloned into the *E. coli* expression vector pET-15b (Novagen) to incorporate an N-terminal hexahistidine tag. The recombinant plasmid was transformed into *E. coli* BL21 (DE3) CodonPlus RIPL (Invitrogen) cells. 10 ml overnight starter culture (100 ml TB with 100 mg l^{-1} ampicillin) was used to inoculate 1 l of the same medium in 2.5 l baffled flasks. Cultures were grown at 310 K and 220 rev min^{-1} to an OD_{600} of ∼3–3.5 and then transferred to 291 K and induced with 0.5 m*M* isopropyl β-D-1-thiogalactopyranoside overnight. Cells were harvested, flash-frozen in liquid nitrogen and stored at 193 K. Thawed cells were resuspended in 10 m*M* HEPES pH 7.5, 0.5 *M* NaCl buffer and lysed by sonication in the presence of 0.5% CHAPS. Cell debris was removed by centrifugation at 3500*g* for 40 min and the supernatant was passed through a DE52 column in the same buffer and loaded onto an Ni^{2+}-chelate affinity column. After extensive washes with buffer containing 25 m*M* imidazole, the protein was eluted with 250 m*M* imidazole, concentrated and subjected to gel filtration on a Superdex 200 26/60 column. Initially, low-salt no-additive buffer (10 m*M* HEPES pH 7.5, 150 m*M* NaCl) was used for final storage to allow the exploration of wider crystallization space. However, FtPth could not be concentrated to above 5 mg ml^{-1} as it precipitated under these conditions. By increasing the ionic strength of the buffer and using Tris–HCl instead of HEPES–Na, the solubility and the protein stability were improved. Glycerol had a detrimental effect. A buffer consisting of 10 m*M* Tris–HCl, 250 m*M* NaCl, 0.2 m*M* TCEP was selected for the final purification step and for the storage of all subsequent protein batches. Fractions containing FtPth were subsequently concentrated, aliquoted, flash-frozen and stored at 193 K.

All samples were subjected to quality control, which included denaturing polyacrylamide gel electrophoresis (SDS–PAGE) and electrospray ionization–time of flight mass spectrometry (ESI–ToF MS). SDS–PAGE did not show additional bands upon loading 15 µg protein. The mass determined by ESI–ToF MS was within the error margin (1 Da) of the expected mass calculated from the sequence and analysis of the remaining ESI–ToF spectra did not reveal the presence of any modified protein species detrimental to crystallization such as partially proteolysed, modified or cross-linked species.

2.2. Crystallization and data collection

Initial crystallization screening was carried out at room temperature using frozen aliquots of protein at concentrations between 5 and 15 mg ml^{-1} in 96-well sitting-drop crystallization trays utilizing various commercially available and internally developed proprietary crystallization screens. Two crystal forms, thin hexagonal plates (50 µm) and thicker nonhexagonal plates, appeared within one week under the same conditions. Suitable crystals for diffraction studies were obtained from a crystallization solution consisting of 25% PEG 3350, 0.2 *M* $MgCl_2$ and 0.1 *M* Bis-Tris pH 6.5 with a protein concentration of 13.8 mg ml^{-1}. Prior to data collection, the crystals were cryoprotected by transferring them to a mixture of ethylene glycol and well solution in a 1:4 volume ratio, soaked for 120 s and flash-frozen at 100 K in a cold nitrogen-gas stream. Diffraction data were collected on a Cu $K\alpha$ rotating-anode X-ray radiation source using an imaging-plate (IP) detector. The crystal diffracted to a resolution limit of 2.25 Å and a complete data set was obtained. The data were processed with *HKL*-2000 (Otwinowski & Minor, 1997) in space group $P2_12_12$, with unit-cell parameters a = 60.7, b = 93.0, c = 33.0 Å. Data-collection statistics are summarized in Table 1.

2.3. Structure determination

The FtPth structure was solved by molecular replacement using the *E. coli* Pth coordinates (PDB entry 2pth; Schmitt *et al.*, 1997) as a search model with the *CCP*4 program suite (Collaborative Computational Project, Number 4, 1994). Alternate cycles of restrained refinement and manual rebuilding in the program *Coot* (Emsley & Cowtan, 2004) completed the structure for residues 2–188. The entire N-terminal hexahistidine tag was not observed. During the last cycles of refinement, water molecules were built automatically into spherical peaks of the $F_o - F_c$ difference electron density and verified by manual inspection. Clear difference densities also appeared for one chloride ion and five ethylene glycol molecules. Table 1 contains a summary of the structure-refinement statistics.

3. Results and discussion

3.1. Overall structure of FtPth

We have established the cloning, expression, purification and crystallization of peptidyl-tRNA hydrolase from *F. tularensis* (FtPth) and determined the crystal structure. Since the C-terminus was found to be disordered in previous Pth structures, the FtPth protein

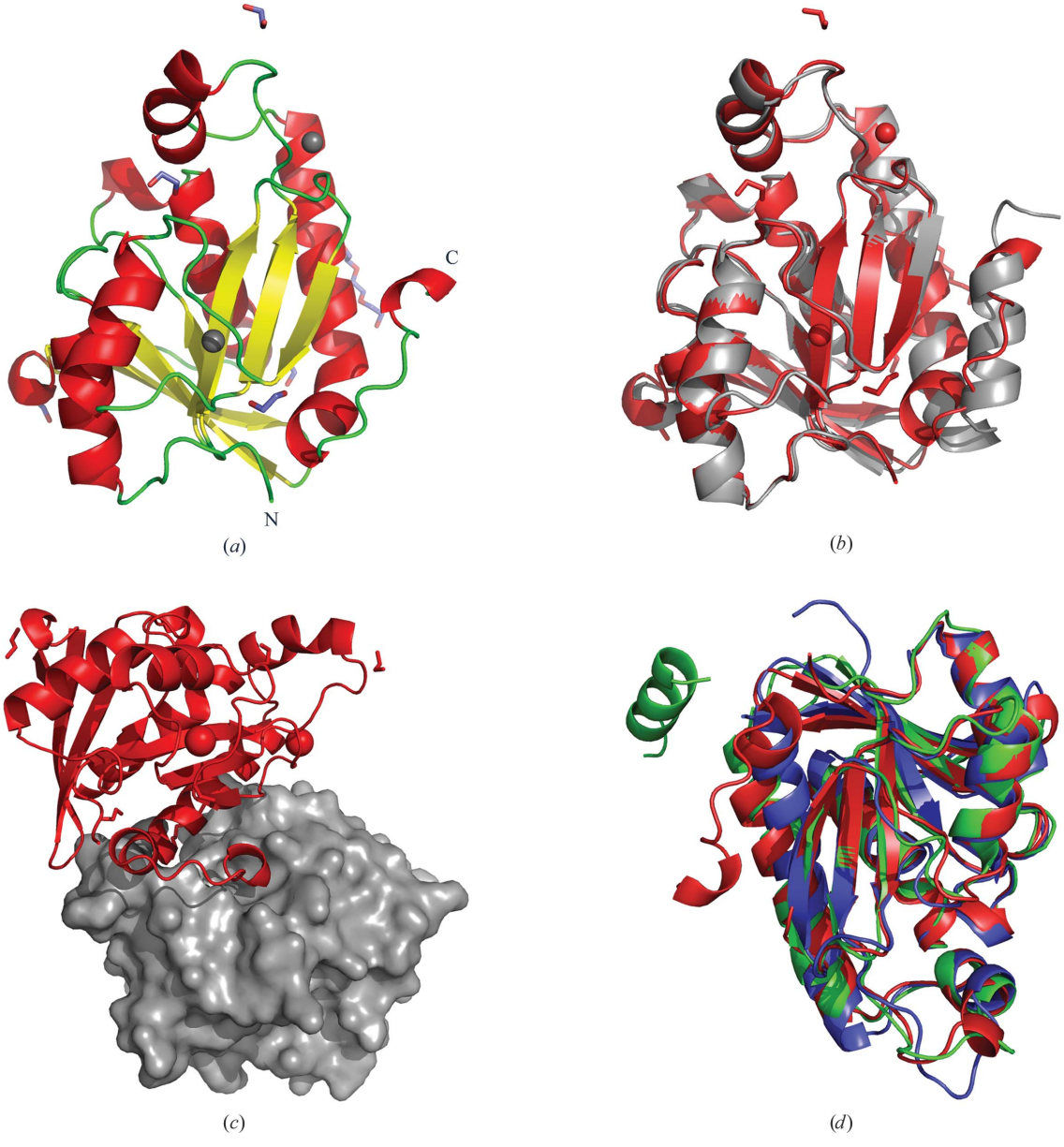

Figure 1
(*a*) Ribbon diagram of the secondary structure of *F. tularensis* peptidyl-tRNA hydrolase (FtPth), with N- and C-termini labeled. The structure comprises a monomer with a single α/β globular domain built around a twisted β-sheet. The coloring scheme for the secondary-structure elements is as follows: α-helices are colored red, β-strands yellow and loops green. Chloride ions are represented by gray spheres, while PEG and ethylene glycol molecules are shown as sticks colored by atom type. (*b*) Superposition with the published *E. coli* structure (PDB entry 2pth). This figure was generated using *PyMOL* (DeLano, 2002). (*c*) Crystal-packing diagram for the *F. tularensis* Pth apo structure. The C-terminus of each molecule (red ribbon) resides in the active site of a neighbouring symmetry mate (gray surface). (*d*) Superposition of the *F. tularensis* (colored red), *E. coli* (colored green; PDB entry 3ofv; R. Lam, T. E. McGrath, V. Romanov, S. A. Gothe, S. R. Peddi, E. Razumova, R. S. Lipman, A. A. Branstrom & N. Y. Chirgadze, unpublished work) and *M. tuberculosis* (colored blue; PDB entry 2z2i; Selvaraj *et al.*, 2007) Pth crystal structures. The core secondary-structure elements and protein fold are conserved in all species. As shown by the superposition, the highly mobile C-terminal helix and adjacent hinge region represent opportunities for designing new constructs (for the identification of feasible crystal forms).

construct was truncated by three residues in an attempt to improve the probability of crystallization. The Ramachandran plot (not shown) indicates 97.3% of residues in the most favored region, 2.2% of residues in allowed regions and 0.5% of residues as outliers. Electron density for the N-terminal residues of the His tag and the terminal Met are missing, probably owing to disorder, and these were not built into the final model, consisting of residues 2–188. In addition, 51 water molecules, a chloride ion and five ethylene glycol molecules were modeled.

FtPth adopts an α/β fold with a twisted seven-stranded β-sheet flanked by helices, similar to other Pth proteins (Figs. 1*a*–1*c*). The mixed β-sheet has four parallel strands flanked by antiparallel strands, with another strand parallel to the central four on the end. The mixed β-sheet is packed between two long α-helices (α1 and α5) and two shorter α-helices (α2 and α3). Another short mobile α-helix (α4) completes the structure. When the crystal packing of FtPth was examined, the C-terminus of each molecule was found to reside within the active site of a neighboring symmetry mate (Fig. 1*c*). The last residue, Leu188, makes contact with the catalytic residue His22 in a symmetry mate.

3.2. Structural differences between FtPth and other Pth-family members

The sequence similarity between FtPth and other Pth-family members was investigated using a *BLAST* search (Altschul *et al.*, 1997). FtPth (gi:3191676) shares 44% sequence identity (84/188) and an *E* value of 4×10^{-34} with *E. coli* Pth (EcPth; gi:157835761), 37% sequence identity (71/190) and an *E* value of 2×10^{-28} with *M. tuberculosis* Pth (MtPth; gi:189095922) and 37% sequence identity (62/166) and an *E* value of 4×10^{-26} with chloroplast group II intron splicing factor Crs2 (CRS2; gi:40889732).

The three-dimensional structure of FtPth was compared with other structures of the Pth family and the structurally similar protein chloroplast RNA-splicing factor 2 (CRS2) from the PDB using the *DALI* server (Holm & Rosenström, 2010). FtPth shows high structural similarity to EcPth (PDB code 2pth, *Z* score 32.6, r.m.s.d. 1.3 Å), CRS2 (PDB code 1ryb, *Z* score 28.5, r.m.s.d. 1.9 Å; PDB code 1ryn, *Z* score 26.3, r.m.s.d. 2.0 Å) and MtPth (PDB code 2z2j, *Z* score 27.6, r.m.s.d. 1.8 Å; PDB code 2jrc, *Z* score 20.3, r.m.s.d. 2.7 Å) (Fig. 1*d*). The core α/β fold of the structures overlay well, but the flexible C-terminus is found in a number of positions. To reduce flexibility in the molecule and possibly improve the ability of these proteins to crystallize, residues from the C-terminus and adjacent hinge region could be deleted as long as there was little detrimental effect on function. The catalytic residue His22 is conserved in all structurally similar structures as well as most of the residues lining the substrate-recognition and catalytically active site, including those in the functionally divergent CRS2 (Ostheimer *et al.*, 2005). This similarity in the active site could be exploited to develop broader spectrum antimicrobial agents.

Peptidyl-tRNA hydrolase is considered to be a good target for antimicrobial agents owing to the differences in sequence and structure between the human and bacterial enzymes. To date, no small-molecule inhibitors for the Pth family of proteins have been discovered even though the enzyme activity and structures of several bacterial Pths have been characterized (Payne *et al.*, 2007). The availability of a variety of protein constructs and crystals of Pth from *F. tularensis* and *E. coli* (unpublished results) enables future studies examining the binding of small molecules by fragment screening, which could be developed into potential inhibitors.

This work was supported by the Transformational Medical Technologies program, contract HDTRA1-06-0041 from the Department of Defense Chemical and Biological Defense program through the Defense Threat Reduction Agency (DTRA). About the Defense Threat Reduction Agency: the Defense Threat Reduction Agency (DTRA) was founded in 1998 to integrate and focus the capabilities of the Department of Defense (DoD) that address the threat by weapons of mass destruction (WMD). DTRA's mission is to safeguard the United States and its allies from chemical, biological, radiological, nuclear and high-yield explosive WMDs by providing capabilities to reduce, eliminate and counter the threat and mitigate its effects. DTRA combines DoD resources, expertise and capabilities to ensure the United States remains ready and able to address present and future WMD threats. For more information on DTRA, visit http://www.dtra.mil. About Transformational Medical Technologies (TMT): TMT was created by DoD to protect the warfighter from emerging and genetically engineered biological threats by discovering and developing a wide range of medical countermeasures through enhanced medical research, development and test and evaluation programs. The TMT Program Office is matrixed from the Joint Science and Technology Office-DTRA and Joint Program Executive Office-Chemical and Biological Defense with oversight from the Office of the Secretary of Defense. For more information on TMT, visit http://www.tmti-cbdefense.org.

References

Altschul, S. F., Madden, T. L., Schäffer, A. A., Zhang, J., Zhang, Z., Miller, W. & Lipman, D. J. (1997). *Nucleic Acids Res.* **25**, 3389–3402.
Brun, G., Paulin, D., Yot, P. & Chapeville, F. (1971). *Biochimie*, **53**, 225–231.
Collaborative Computational Project, Number 4 (1994). *Acta Cryst.* D**50**, 760–763.
DeLano, W. L. (2002). *PyMOL.* http://www.pymol.org.
De Pereda, J. M., Waas, W. F., Jan, Y., Ruoslahti, E., Schimmel, P. & Pascual, J. (2004). *J. Biol. Chem.* **279**, 8111–8115.
Emsley, P. & Cowtan, K. (2004). *Acta Cryst.* D**60**, 2126–2132.
Fromant, M., Schmitt, E., Mechulam, Y., Lazennec, C., Plateau, P. & Blanquet, S. (2005). *Biochemistry*, **44**, 4294–4301.
Goodall, J. J., Chen, G. J. & Page, M. G. (2004). *Biochemistry*, **43**, 4583–4591.
Holm, L. & Rosenström, P. (2010). *Nucleic Acids Res*, **38**, W545–W549.
Kössel, H. (1970). *Biochim. Biophys. Acta*, **204**, 191–202.
Meinnel, T., Mechulam, Y. & Blanquet, S. (1993). *Biochimie*, **75**, 1061–1075.
Menez, J., Buckingham, R. H., de Zamaroczy, M. & Campelli, C. K. (2002). *Mol. Microbiol.* **45**, 123–129.
Menninger, J. R. (1976). *J. Biol. Chem.* **251**, 3392–3398.
Menninger, J. R. (1979). *J. Bacteriol.* **137**, 694–696.
Ostheimer, G. J., Hadjivassiliou, H., Kloer, D. P., Barkan, A. & Matthews, B. W. (2005). *J. Mol. Biol.* **345**, 51–68.
Otwinowski, Z. & Minor, W. (1997). *Methods Enzymol.* **276**, 307–326.
Oyston, P., Sjostedt, A. & Titball, R. (2004). *Nature Rev. Microbiol.* **2**, 967–978.
Payne, D. J., Gwynn, M. N., Holmes, D. J. & Pompliano, D. L. (2007). *Nature Rev. Drug Discov.* **1**, 29–40.
Pulavarti, S. V. S. R. K., Jain, A., Pathak, P. P., Mahmood, A. & Arora, A. (2008). *J. Mol. Biol.* **378**, 165–177.
Rosas-Sandoval, G., Ambrogelly, A., Rinehart, J., Wei, D., Cruz-Vera, L. R., Graham, D. E., Stetter, K. O., Guarneros, G. & Söll, D. (2002). *Proc. Natl Acad. Sci. USA*, **99**, 16707–16712.
Schmitt, E., Mechulam, Y., Fromant, M., Plateau, P. & Blanquet, S. (1997). *EMBO J.* **16**, 4760–4769.
Selvaraj, M., Roy, S., Singh, N. S., Sangeetha, R., Varshney, U. & Vijayan, M. (2007). *J. Mol. Biol.* **372**, 186–193.